Electrochemical Performances of MnO_2 Impregnated Activated Carbon from Vetiver Root Waste

Raden Roro Nisrina DSP Pargustan[1], Ratna Frida Susanti[2], Haryo Satriya Oktaviano[3], Arenst Andreas Arie[4], Agung Nugroho[5]

{102318038@student.universitaspertamina.ac.id[1], santi@unpar.ac.id[2], haryo.oktaviano@pertamina.com[3], arenst@unpar.ac.id[4], agung.n@universitaspertamina.ac.id[5]}

Department of Chemical Engineering, Faculty of Industrial Technology, Universitas Pertamina, Jakarta, Indonesia[1,5], Chemical Engineering Department, Industrial Technology Faculty, Parahyangan Catholic University, Bandung, Indonesia[2,4], Research and Technology Innovation, PT. Pertamina (Persero), Jakarta, Indonesia[3]

Abstract. Vetiver root waste from distillation of essential oil is high in cellulose, hemicellulose, and lignin, making it an excellent precursor for porous activated carbon. High-temperature pyrolysis, KOH activation, and a hydrothermal approach were used to produce activated carbon. X-ray diffraction (XRD), Fourier-transform infrared (FTIR), and Raman spectroscopy were used to investigate its properties. The results showed that MnO2 impregnation affected the carbon structure. A three-electrode arrangement with Ag/AgCl and Pt wire was used for electrochemical measurements. At a current density of 1 A/g, the calculated specific capacitance of porous activated carbon has been found to be 218 F/g. At the same current density, the specific capacitance increased considerably after MnO2 impregnation to 443 F/g. This improvement highlights the potential of MnO2-impregnated activated carbon as electrodes for supercapacitors.

Keywords: Impregnation, Vetiver root waste, Manganese dioxide, Activated carbon, Galvanostatic charge-discharge

1 Introduction

The growing focus on digital transformation in all disciplines necessitates a supply of electrical energy as one of the primary energy sources in the Industry 4.0 era. To address this, there are increasing demands for developing electrical energy storage devices that are more compact, have a larger storage capacity, are less expensive, and have better durability. [1].

There has been a rise in demand for clean, environmentally friendly energy as a substitute for fossil fuels in recent years. Solar, wave, geothermal, wind, and other clean and renewable energy sources necessitate using energy storage systems. Renewable energy development is believed to depend on the availability and usability of existing energy storage devices. Energy storage devices include supercapacitors and batteries [2]. Supercapacitors are among the

ICO-SEID 2022, November 23-24, Jakarta, Indonesia

DOI 10.4108/eai.23-11-2022.2339149

interesting ones that researchers continue to develop. This is due to their advantages in having high power density, wide operating temperature range, good recyclability, low internal resistance, and high efficiency [3], [4]. Supercapacitor research has focused on carbon-based electrodes because of their abundance, low cost, and high electrical conductivity [5].

Improving the electrochemical properties of activated carbon has become one of the recent subjects of research for use as supercapacitor electrodes. This can be done by adding metal oxide in the electrode material. Recent studies have demonstrated that metal oxides have higher theoretical capacitance compared to activated carbon [6]. The coupling of metal oxide with activated carbon enhances the electrochemical characteristics of supercapacitators' electrodes utilizing high-theoretical capacitance of metal oxide and a large surface area provided by the activated carbon [7]. A research conducted by Zhou in 2019, added MnO_2 metal to activated carbon from sugarcane bagasse using the hydrothermal method and obtained an increase in specific capacitance from 89 F/g to 492.5 F/g at a current density of 1 A/g [8]. Zhou [9] modified activated carbon from tea shell oil by adding MnO_2 using stirring method and found an increase in specific capacitance from 146 F/g to 1126 F/g at 0.5 A/g thanks to the active sites of MnO_2. Li [10] also succeeded in synthesizing MnO_2/activated carbon made from rambutan peel using the hydrothermal method which was then arranged into an asymmetric capacitor and obtained a capacitance of 137 F/g at a current density of 0.5 A/g.

In this study, activated carbon were synthesized from vetiver root waste. The impregnation of manganese dioxide into the carbon structure was carried out by hydrothermal method. The morphology, functional groups, and crystal structure of the material were tested using XRD, Raman and FTIR. As well as electrochemical technique which included cyclic voltammetry (CV) and galvanostatic charge-discharge (GCD) to understand the material's potential for supercapacitor electrode application.

2 Materials and Method

Materials. Potassium hydroxide (KOH) from Merck, Potassium permanganate (KMnO4) from SAP Chemical, Sodium hydroxide (NaOH) from Merck, Sulfuric acid (H2SO4) from Mallinckrodt, and Nafion from Merck were employed. All the reagents used were of analytical grade.

Synthesis of Activated Carbon. First, the vetiver root waste was cleaned with water to eliminate contaminants before being dried in an oven at 110°C for 24 hours. The dried powder was then ball-milled and sieved to 100 mesh. The resulting powder then pre-carbonized in muffle furnace at 400°C for 1 h which can be called pre-carbonized powder [11]. This powder was mixed with KOH pellet using mortar at ratio KOH/C = 3:1. The activation process was done at 800°C for 2 h in nitrogen atmosphere to obtain the VRW-AC samples.

Synthesis of MnO_2/Activated Carbon. The MnO_2 - actived carbon composite (VRW-ACM MnO_2) was synthesized using hydrothermal process. In this process, a 0.02 g $KMnO_4$ powder was dissolved in 160 ml of double-distilled water, followed by the dispersion of 0.1 g of vetiver root waste activated carbon (VRW-AC) in the KMnO4 solution. The mixture was

stirred for 30 minutes. The mixture was then placed in a 200 mL teflon-lined autoclave and heated to 150°C using oven. After 24 h of hydrothermal reaction, the mixture was washed multiple times using double distilled water and dried in the vacuum oven at 70°C for 8 h, and the VRW-ACM MnO_2 sample was obtained.

Characterization. FTIR analysis was obtained using Thermo Scientific iS 5 in the range wavelengths of 600-4000 cm^{-1} to investigate functional groups. The crytalinity of the samples was identified using X-Ray Diffraction on an Olympus BTX II Benchtop with Co-K radiation (= 0.17902 nm) at 0.5°/min scan rate. Horiba spectrometer (LabRAM HR Evolution Raman Microscope) was employed to determine Raman spectra at an excitation of 532 nm and grating 1800 g/mm.

Electrochemical Measurement. Working electrode in this experiment was prepare by coating ink of active material into a glassy carbon electrode. The ink was created by combining 1.6 mg of active material (AC or MnO2/AC) with 0.5 ml of isopropanol and sonicating it for 15 minutes [12], [13]. With the aid of 0.3 µl nafion, 0.6 µl ink was deposited onto a glassy carbon surface. The three-electrode system was constructed using the above mention working electrode, Pt wire counter electrode, Ag/AgCl reference electrode, and 1 M Na_2SO_4 aqueous solution as an electrolyte. CV measurement was performed at rates ranging from 5 to 100 mV/s while GCD measurement ranged from 0.5 to 4 A/g.

3 Results and Discussion

Characterization. For all synthesized materials, the FTIR analysis results given in Figure 1 show notable peaks at wavenumbers 1636, 2922, and 3444 cm^{-1}. These peaks correspond to the O-H stretching, C-H stretching, and C=C stretching functional groups, respectively. The existence of the O-H functional group, as indicated by the peak at 3444 cm^{-1}, indicates the presence of the O-H bond, which is often present in activated carbon [14]. he presence of oxygen functional groups in the sample could improves conductivity when used as a supercapacitor electrode [15]. A prominent Mn-O stretch is found in the wavenumber range of 650-600 cm^{-1} for ACM-MnO_2 samples, demonstrating the successful impregnation of MnO2 in activated carbon [16], [17].

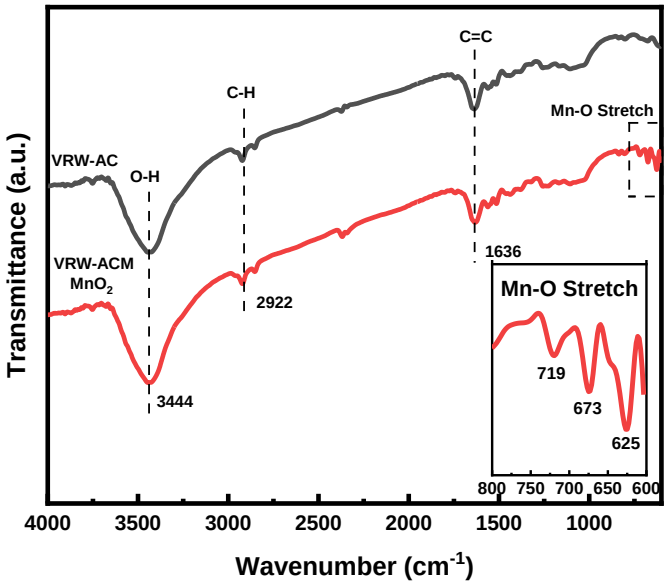

Fig. 1. FTIR spectra for VRW-ACM and VRW-ACM-MnO_2

Figure 2 shows that Raman test exhibits bands 1340 cm^{-1} (D-band) and 1578 cm^{-1} (G-band). The D-Band describes the level of amorphous and lattice distortion in the sample while the G-Band describes the level of graphitization [15].

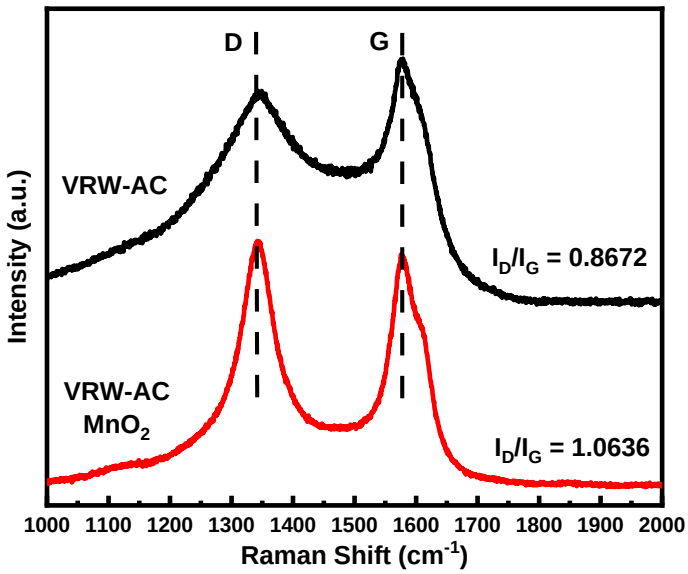

Fig. 2. Raman Spectra of the activated carbon from vetivier root waste and the composite of MnO2-AC

The defect degree in VRW-ACM/MnO_2 and VRW-ACM was quantified through the comparison between intensities of the D-band and G-band (see Table 1).

Table 1. Raman Spectra and calculated intensity ratio of D-Band and G-Band

Sample Name	D-Band		G-Band		I_D/I_G
	Raman Shift (cm^{-1})	Intensity (a.u)	Raman Shift (cm^{-1})	Intensity (a.u)	
VRW-ACM	1349.09	0.8583	1578.77	0.9898	0.8672
VRW-ACM/MnO_2	1342.08	0.9980	1578.35	0.9408	1.0608

Structural defects increase after the metal impregnation process. Thus, the ID/IG value of the VRW-ACM becomes lower than that of VRW-ACM/MnO_2. The increase in the I_D/I_G parameter is due to the oxidation process which leads to the formation of MnO2 from KMnO4 and the carbons, resulting in a carbon materials structure destruction [18]. Moreover, the increase in I_D/I_G may be due to MnO_2-activated carbon bonds held together by oxygen [19].

In this study, the results of the Raman spectroscopy test showed agreement with previous studies [19]–[21]. This shows that the degree of graphitization is lower and the degree of amorphous carbon is higher.

In the XRD test in **Figure 3**, it can be seen that the VRW-ACM samples show peaks at 26.58° and 44.26°. Those peaks indicate porous carbon material and are commonly found in activated carbon [22]. After the MnO_2 impregnation process, it was seen that there were additional peaks at 31.22° and 37.92°. Those peaks correspond to MnO_2 [23]. So it can be said that the MnO_2 impregnation process has been successfully carried out. All MnO_2 peaks show a weak intensity which indicates that the MnO_2 formed on activated carbon material has low crystallinity and advantageous to increase the capacitance of the material [24].

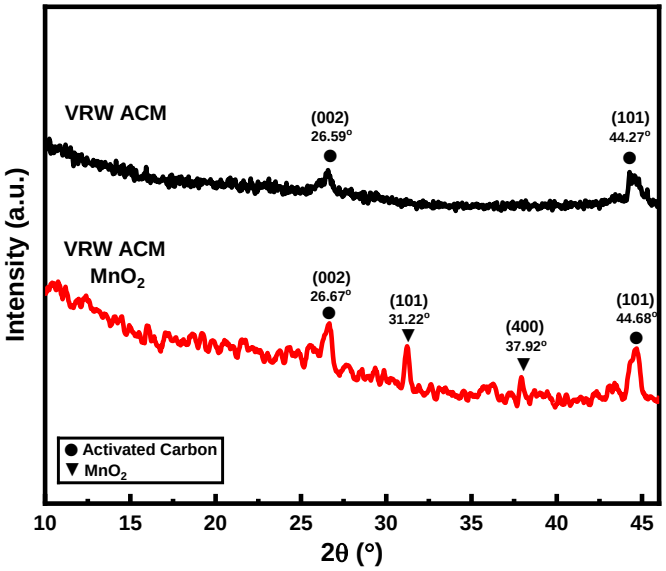

Fig. 3. XRD Test Result for VRW-ACM and VRW-ACM-MnO_2

Electrochemical Measurement. The CV graph in **Figure 4** for the VRW-ACM sample has a symmetrical rectangular form, revealing the storage mechanism of the Electric Double Layer Capacitor (EDLC). The adsorption and desorption of Na^+ ions from the electrolyte are involved in EDLC storage, which is a reversible surface phenomenon. The shape of the CV graph no longer forms a square in samples impregnated with MnO_2 because of a redox reaction between electrolyte ions and MnO_2, which is a feature of the pseudocapacitance mechanism [6].

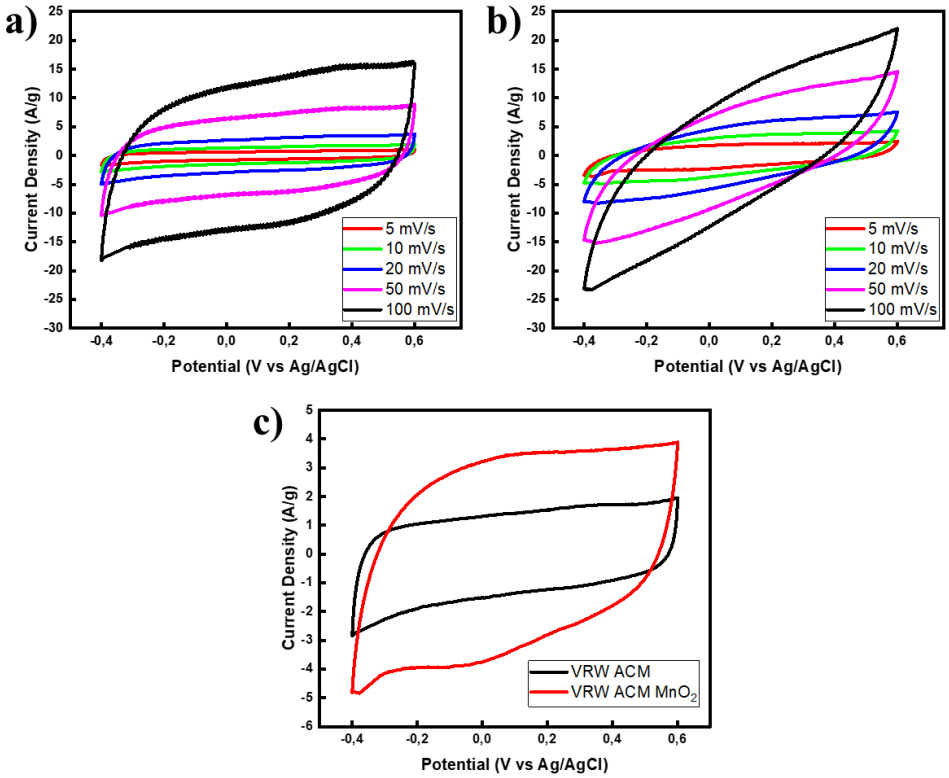

Fig. 4. CV test result for (a)VRW-ACM (b)VRW-ACM-MnO_2 and (c)comparison at scan rate 10 mV/s

When comparing CV test findings for VRW-ACM and VRW-ACM-MnO2 samples, the area of the curve for the VRW ACM MnO2 samples has risen. This demonstrates that the addition of metal oxides can increase the capacitance of the material due to the combination of the porous activated carbon material's EDLC storage mechanism and the pseudocapacitance mechanism of the impregnated metal oxide into activated carbon [6].

Figure 5 shows the GCD test for the VRW ACM sample, and the curve forms a triangle shape. This shape represents the EDLC process that occurs [6]. Meanwhile, the two MnO2-impregnated samples use a combination of EDLC and pseudocapacitance. This is demonstrated by the triangle form in the GCD test, which has a distortion that results in a larger triangular area with a longer discharge time [25]. The distortion indicates a redox interaction between electrolyte ions and MnO_2.

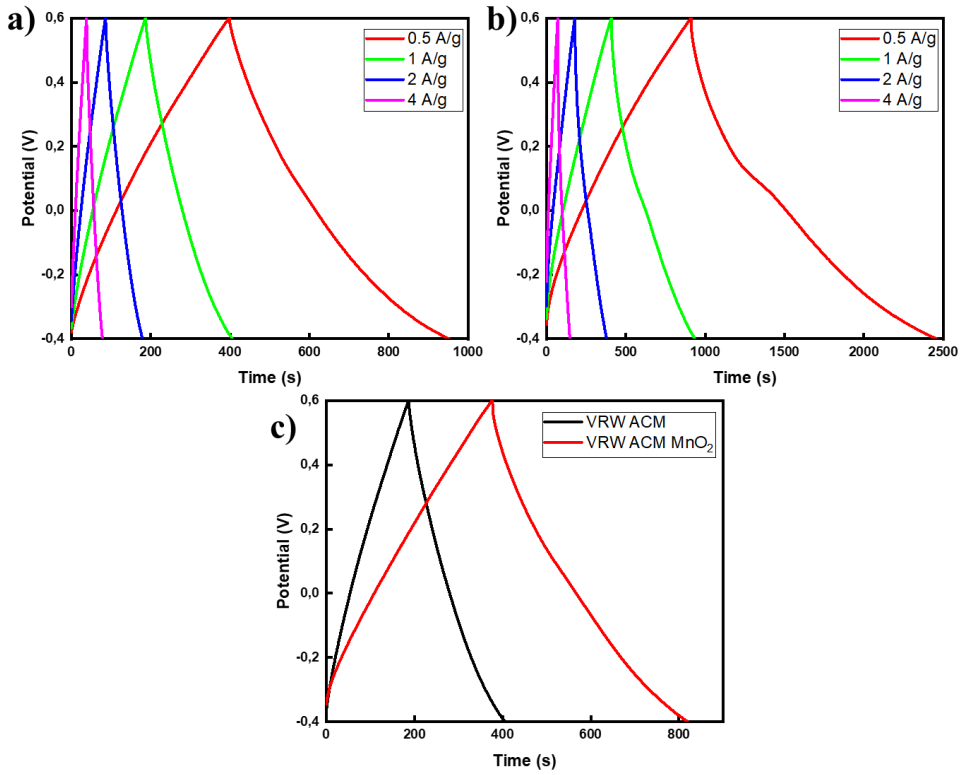

Fig. 5. GCD test result for (a)VRW-ACM, (b)VRW-ACM-MnO_2 and (c)comparison at current density 1A/g

Specific capacitance were calculated using equation (1)

$$C_m = \frac{I\,\Delta t}{m\,\Delta V} \tag{1}$$

where, Δt is discharge time (s), I is current (A), ΔV is potential window (V) and m is sample mass applied on working electrode (g). The result as shown in Table 2.

Table 2. Capacitance Curve from GCD for activated carbon derived from vetivier root waste

Sample	Current Density (A/g)	Specific Capacitance (F/g)	Increase of Capacitance
VRW AC	0.5	277	-
	1	218	-
	2	186	-
	4	160	-
VRW ACM MnO_2	0.5	590.5	113.18%
	1	443	103.21%
	2	368	97.85%
	4	308	92.5%

The synergistic effect of the metal oxide and carbon material was responsible for the increase in specific capacitance value after MnO2 impregnation. Metal oxides with large theoretical capacitance values filled the pores of the carbon material, providing additional active sites for redox processes [6]. MnO2 can react reversibly in electrochemical processes, improving the material's electrochemical performance [10].

4 Summary

Vetiver waste from the essential oil distillation process can be used as a precursor for synthesizing activated carbon by pyrolysis processes, with KOH acting as an activator. The characterization test findings suggest that the manganese dioxide addition into the activated carbon material was successful. The presence of the Mn-O functional group in the FTIR test, an increasing degree of irregularity or defect in the Raman Spectroscopy test, and the appearance of manganese dioxide peaks in the XRD test all support this. Manganese dioxide was used to increase the electrochemical performance of the produced activated carbon material. The specific capacitance of VRW-ACM increases from 218 to 443 F/g with cycle retention of 93.49% following MnO_2 impregnation.

References

[1] J. Elio, P. Phelan, R. Villalobos, and R. J. Milcarek, "A review of energy storage technologies for demand-side management in industrial facilities," *J. Clean. Prod.*, vol. 307, p. 127322, Jul. 2021, doi: 10.1016/J.JCLEPRO.2021.127322.

[2] K. Mensah-Darkwa, C. Zequine, P. K. Kahol, and R. K. Gupta, "Supercapacitor Energy Storage Device Using Biowastes: A Sustainable Approach to Green Energy," *Sustain. 2019, Vol. 11, Page 414*, vol. 11, no. 2, p. 414, Jan. 2019, doi: 10.3390/SU11020414.

[3] G. L. Bullard, H. B. Sierra-Alcazar, H. L. Lee, and J. L. Morris, "Operating principles of the ultracapacitor," *IEEE Trans. Magn.*, vol. 25, no. 1, pp. 102–106, 1989, doi: 10.1109/20.22515.

[4] L. Zhang, X. Hu, Z. Wang, F. Sun, and D. G. Dorrell, "A review of supercapacitor modeling, estimation, and applications: A control/management perspective," *Renew. Sustain. Energy Rev.*, vol. 81, pp. 1868–1878, Jan. 2018, doi: 10.1016/J.RSER.2017.05.283.

[5] E. Frackowiak, Q. Abbas, and F. Béguin, "Carbon/carbon supercapacitors," *J. Energy Chem.*, vol. 22, no. 2, pp. 226–240, Mar. 2013, doi: 10.1016/S2095-4956(13)60028-5.

[6] H. Shen, X. Kong, P. Zhang, X. Song, H. Wang, and Y. Zhang, "In-situ hydrothermal synthesis

of δ-MnO2/soybean pod carbon and its high performance application on supercapacitor," *J. Alloys Compd.*, vol. 853, p. 157357, Feb. 2021, doi: 10.1016/J.JALLCOM.2020.157357.
[7] S. Kong *et al.*, "MnO2 nanosheets decorated porous active carbon derived from wheat bran for high-performance asymmetric supercapacitor," *J. Electroanal. Chem.*, vol. 850, p. 113412, Oct. 2019, doi: 10.1016/J.JELECHEM.2019.113412.
[8] B. Zhou *et al.*, "Synthesis of Ultrathin MnO2 Nanosheets/Bagasse Derived Porous Carbon Composite for Supercapacitor with High Performance," *J. Electron. Mater. 2019 485*, vol. 48, no. 5, pp. 3026–3035, Feb. 2019, doi: 10.1007/S11664-019-07019-7.
[9] M. Zhou, J. Gomez, B. Li, Y. B. Jiang, and S. Deng, "Oil tea shell derived porous carbon with an extremely large specific surface area and modification with MnO2 for high-performance supercapacitor electrodes," *Appl. Mater. Today*, vol. 7, pp. 47–54, Jun. 2017, doi: 10.1016/J.APMT.2017.01.008.
[10] M. Li, J. Yu, X. Wang, and Z. Yang, "3D porous MnO2@carbon nanosheet synthesized from rambutan peel for high-performing supercapacitor electrodes materials," *Appl. Surf. Sci.*, vol. 530, p. 147230, Nov. 2020, doi: 10.1016/J.APSUSC.2020.147230.
[11] R. Chaudhary *et al.*, "Removal of Oil and Grease in Wastewater using Palm Kernel Shell Activated Carbon," *IOP Conf. Ser. Earth Environ. Sci.*, vol. 549, no. 1, p. 012064, Aug. 2020, doi: 10.1088/1755-1315/549/1/012064.
[12] R. E. Haraki, A. A. Arie, R. F. Susanti, H. S. Oktaviano, and A. Nugroho, "Synthesis and Electrochemical Properties of ZnO/ Activated Carbon from Vetiver Distillation Waste," *Eng. Chem.*, vol. 2, pp. 35–41, 2023, doi: 10.4028/p-1z7h01.
[13] A. Nugroho *et al.*, "Synthesis and Characterization NS-Reduced Graphene Oxide Hydrogel and Its Electrochemical Properties," *Lett. Mater.*, vol. 12, no. 2, pp. 169–174, 2022, doi: 10.22226/2410-3535-2022-2-169-174.
[14] M. Danish *et al.*, "Comparison of surface properties of wood biomass activated carbons and their application against rhodamine B and methylene blue dye," *Surfaces and Interfaces*, vol. 11, pp. 1–13, Jun. 2018, doi: 10.1016/J.SURFIN.2018.02.001.
[15] E. Elaiyappillai *et al.*, "Low cost activated carbon derived from Cucumis melo fruit peel for electrochemical supercapacitor application," *Appl. Surf. Sci.*, vol. 486, pp. 527–538, Aug. 2019, doi: 10.1016/J.APSUSC.2019.05.004.
[16] C. M. Julien, M. Massot, and C. Poinsignon, "Lattice vibrations of manganese oxides: Part I. Periodic structures," *Spectrochim. Acta Part A Mol. Biomol. Spectrosc.*, vol. 60, no. 3, pp. 689–700, Feb. 2004, doi: 10.1016/S1386-1425(03)00279-8.
[17] S. J. Parikh and J. Chorover, "FTIR Spectroscopic Study of Biogenic Mn-Oxide Formation by Pseudomonas putida GB-1," *https://doi.org/10.1080/01490450590947724*, vol. 22, no. 5, pp. 207–218, Jul. 2007, doi: 10.1080/01490450590947724.
[18] L. Ma, D. Li, L. Wang, and X. Ma, "In situ hydrothermal synthesis of α-MnO2 nanowire/activated carbon hollow fibers from cotton stalk composite: dual-effect cyclic visible light photocatalysis performance," *Cellul. 2020 2715*, vol. 27, no. 15, pp. 8937–8948, Aug. 2020, doi: 10.1007/S10570-020-03405-1.
[19] N. L. Tuyen, P. Q. Trieu, N. N. Dinh, N. T. Trung, and D. Van Thanh, "Synthesis of MnO2/Graphene Nanocomposites using Plasma Electrolysis Method for Photocatalytic Degradation of Methyl Orange Dye in Water," *VNU J. Sci. Math. - Phys.*, vol. N38, no. 2, pp. 55–61, Jun. 2022, doi: 10.25073/2588-1124/VNUMAP.4679.
[20] H. Shen *et al.*, "Facile hydrothermal synthesis of actiniaria-shaped α-MnO2/activated carbon and its electrochemical performances of supercapacitor," *J. Alloys Compd.*, vol. 770, pp. 926–933, Jan. 2019, doi: 10.1016/J.JALLCOM.2018.08.228.
[21] T. Yumak, "Electrochemical Performance of Fabricated Supercapacitors Using MnO2/Activated Carbon Electrodes," *Hacettepe J. Biol. Chem.*, vol. 47, no. 1, pp. 115–122, 2019.
[22] J. Xu, L. Chen, H. Qu, Y. Jiao, J. Xie, and G. Xing, "Preparation and characterization of activated carbon from reedy grass leaves by chemical activation with H3PO4," *Appl. Surf. Sci.*, vol. 320, pp. 674–680, Nov. 2014, doi: 10.1016/J.APSUSC.2014.08.178.
[23] U. Kamran, Y. J. Heo, J. W. Lee, and S. J. Park, "Chemically modified activated carbon

decorated with MnO2 nanocomposites for improving lithium adsorption and recovery from aqueous media," *J. Alloys Compd.*, vol. 794, pp. 425–434, Jul. 2019, doi: 10.1016/J.JALLCOM.2019.04.211.

[24] S. Xiong *et al.*, "Hydrothermal synthesis of high specific capacitance electrode material using porous bagasse biomass carbon hosting MnO2 nanospheres," *Biomass Convers. Biorefinery 2019 114*, vol. 11, no. 4, pp. 1325–1334, Nov. 2019, doi: 10.1007/S13399-019-00525-Y.

[25] V. Sannasi and K. Subbian, "Influence of Moringa oleifera gum on two polymorphs synthesis of MnO2 and evaluation of the pseudo-capacitance activity," *J. Mater. Sci. Mater. Electron. 2020 3119*, vol. 31, no. 19, pp. 17120–17132, Aug. 2020, doi: 10.1007/S10854-020-04272-Z.